STAR JPSS

Monthly Newsletter

September 2016

A note from the Program Manager: Welcome to the new STAR JPSS Monthly Newsletter. September was a busy month for the STAR JPSS Program. STAR OMPS NP V8Pro DAP was delivered to NDE on Sept 30th 2016. STAR ASSIST and land teams completed critical design reviews for surface reflectance, LST & Albedo, Vegetation Indexes algorithms. The surface albedo team supported a LUT update in operation. The aerosol team organized a two-day workshop on September 13-14, 2016 and conducted briefings and interactive hands-on tutorials for science and operational users. STAR SDR/EDR teams also provided extensive independent assessments of the JPSS Block 2.0 testing and the results were reported back to the JPSS program as part of the JPSS-1 Cal Val Readiness.

Program Highlights

Imagery – VIIRS DNB images have been made showing likely power outages associated with the deadly 6.2M earthquake that impacted central Italy on August 24, 2016). Before and after images highlighting Amatrice are shown in the figure below. The town of Amatrice suffered significant damage according to reports (http://www.bbc.com/news/world-europe-37176601) and the earthquake was responsible for more than 250 fatalities. Additional images were created using a variety of display software to determine their strengths and weaknesses related to the visibility of small scale power outages.

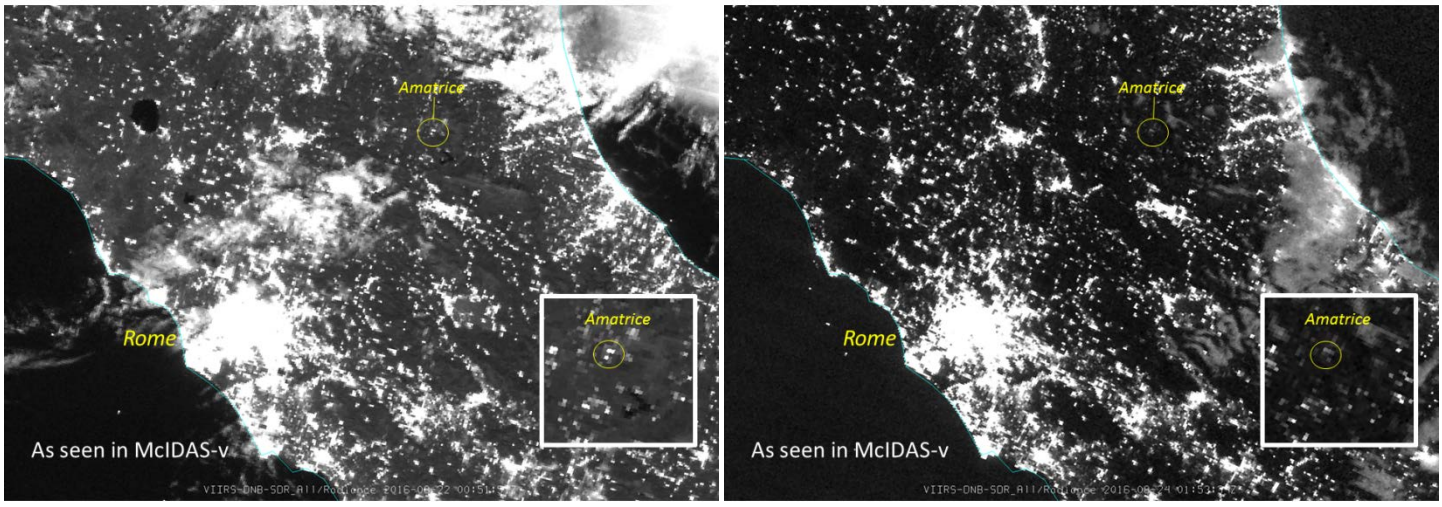

Figure 1. VIIRS DNB images of central Italy from before the earthquake (00:52 UTC 22 August 2016; top) and after the earthquake (01:53 UTC 24 August 24, 2016; bottom). The insets show the appearance of Amatrice, a town which suffered significant damage. The reduction in brightness of the pixels in and around Amatrice indicates a power outage has occurred.

Imagery - The VIIRS Imagery team has provided the following image as an "Image of the Month" for the STAR JPSS website. The image shows Hurricane Lester, spinning in the east Pacific, which reached

its peak intensity of 120 kts on the afternoon of August 29, 2016. VIIRS passed over near that time and collected these full resolution 375 m images. The large image is from band I5 (infrared), and the inset is the corresponding I1 (visible).

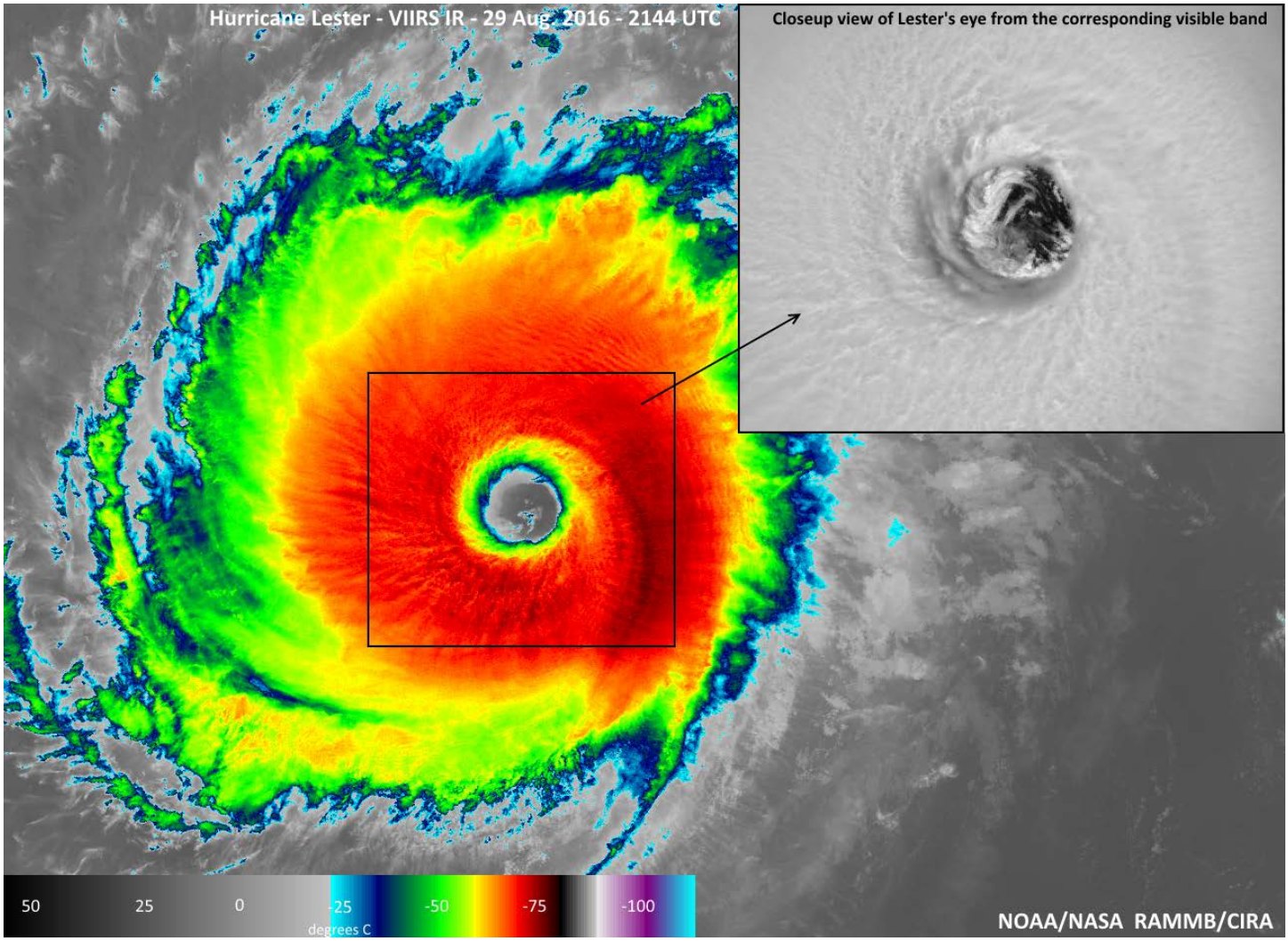

Figure 2. Hurricane Lester, spinning in the east Pacific, which reached its peak intensity of 120 kts on the afternoon of August 29, 2016.

Upcoming Events

- Asia-Oceania Meteorological Satellite Users' Conference (Oct. 21-28, Incheon, Korea),
- GOFC-GOLD Fire Implementation Team meeting and Forest Sat 2016 Conference (Nov. 15-17, Santiago, Chile)
- AGU Fall Meeting (Dec 12-16, San Francisco, CA)
- AMS Annual Meeting (Jan 22-25, Seattle, WA)

Publications

Aerosols - A manuscript entitled "An enhanced VIIRS aerosol optical thickness (AOT) retrieval algorithm over land using a global surface reflectance ratio database" by STAR aerosol team has been accepted for publication in *JGR-Atmospheres*. This manuscript describes a new approach to derive aerosol optical depth over bright surfaces that is currently not possible with the operational IDPS algorithm. The code for this

algorithm along with other updates has been delivered to AIT team for testing and implementation within the NDE operational environment. Co-authors: Hai Zhang (IMSG), Shobha Kondragunta (STAR), Istvan Laszlo (STAR), Hongqing Liu (IMSG), Lorraine Remer (UMBC), Jingfeng Huang (UMD-CICS), Stephen Superczynski (SRG), and Pubu Ciren (IMSG).

NUCAPS – A manuscript summarizing the performance of the NUCAPS atmospheric vertical moisture profile product in the vicinity of atmospheric rivers and Saharan air layers using data acquired from the 2015 CalWater/ACAPEX and AEROSE campaigns has been accepted as an Expedited Contribution (pending minor revisions) in the *Journal of Hydrometeorogy.*

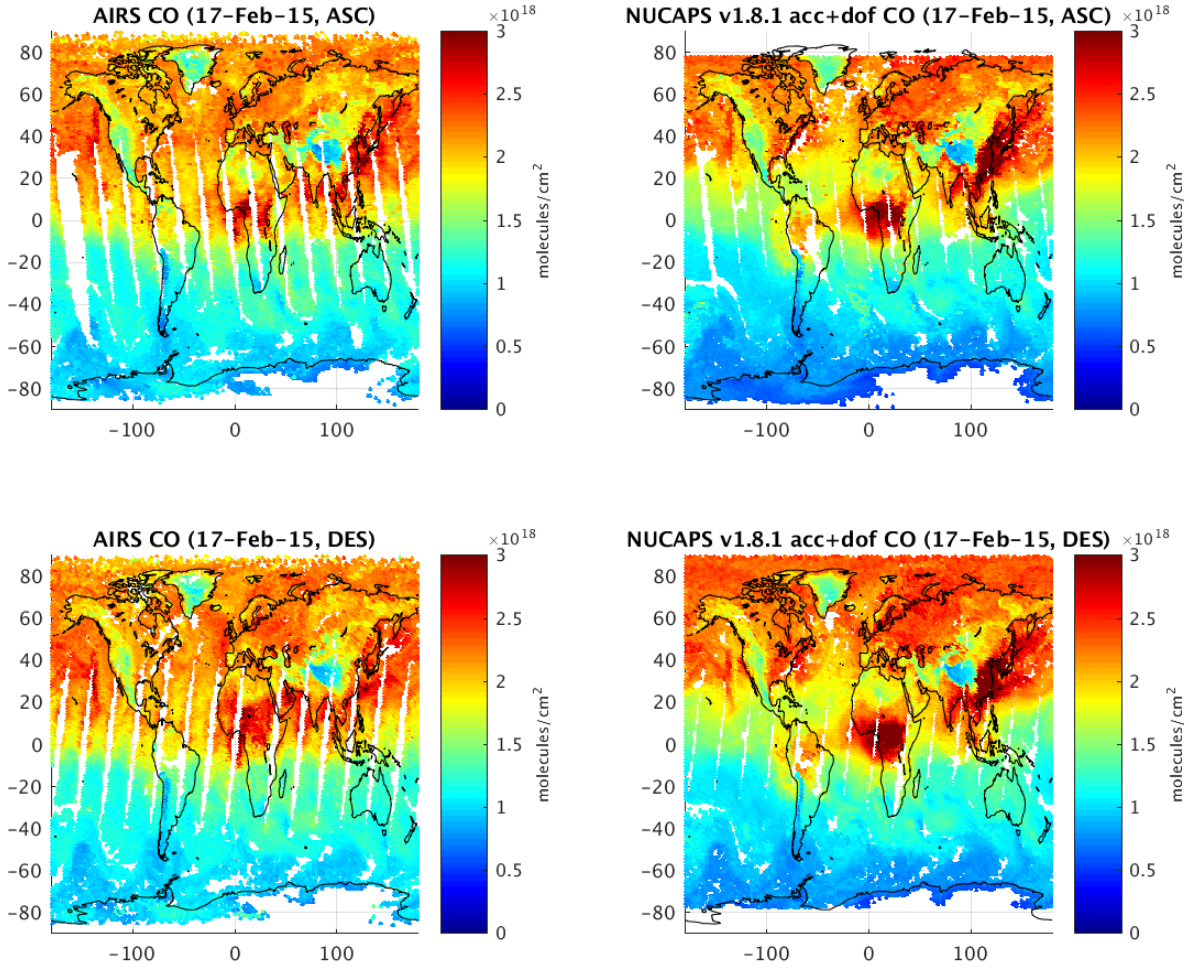

Figure 3. Carbon monoxide for ascending (top) and descending (bottom) orbits from AIRS (left) and NUCAPS (right).

Cryosphere - A paper titled "Comparison of sea ice thickness from satellites, aircraft, and PIOMAS data" was recently published in the journal Remote Sensing (2016, 8, 713, doi:10.3390/rs8090713). The paper, by Xuanji Wang (CIMSS), Jeff Key (STAR), Ron Kwok (NASA JPL), and Jinlun Zhang (University of Washington), compares Arctic sea ice thickness from the APP-x using the algorithm developed for the VIIRS, the ICESat laser altimeter, the CryoSat-2 radar altimeter, the IceBridge aircraft campaign laser altimeter and snow radar, the SMOS sensor, and the PIOMAS ice model. All satellite-retrieved ice thickness products and PIOMAS overestimate the thickness of thin ice (1 m or less) compared to IceBridge. The spatial correlation between the datasets indicates that APP-x and PIOMAS are the most similar, followed by APP-x and CryoSat-2.

Ocean Color - An implementation approach using the OCI-based Chl-a algorithm for the Suomi NPP VIIRS has been developed. The OCI Chl-a algorithm for satellite-derived Chl-a data was originally developed by *Hu et al.* (2012) (J. Geophys. Res., 117, C01011, doi: 01010.01029/02011JC007395) for MODIS. It uses two Chl-a algorithms, i.e., the CI-based (reflectance difference-based) algorithm for oligotrophic waters and the usual OCx-based (reflectance ratio-based) algorithm (e.g., OC3M for MODIS and OC3V for VIIRS), and merges the two algorithms for different Chl-a range applications (named OCI algorithm). In this study, we use the in situ MOBY optics data to demonstrate conclusively that using the CI-based Chl-a algorithm can significantly improve VIIRS Chl-a data over oligotrophic waters with much reduced data noise from instrument calibration and the imperfect atmospheric correction. Using the VIIRS-measured global Chl-a data derived from the MSL12 ocean color data processing system, we have developed the CI-based algorithm specifically for VIIRS, and further improved the two Chl-a algorithms merging method using the blue-green reflectance ratio values. Extensive evaluation results show that the new OCI Chl-a algorithm for VIIRS can produce consistent Chl-a data compared with those from the OC3V algorithm. In particular, the data transition between the CI-based and OC3V-based Chl-a algorithm is quite smooth, and there are no obvious discontinuities in VIIRS-derived Chl-a data. The new OCI-based Chl-a algorithm has been implemented in MSL12 for routine production of VIIRS global Chl-a data.

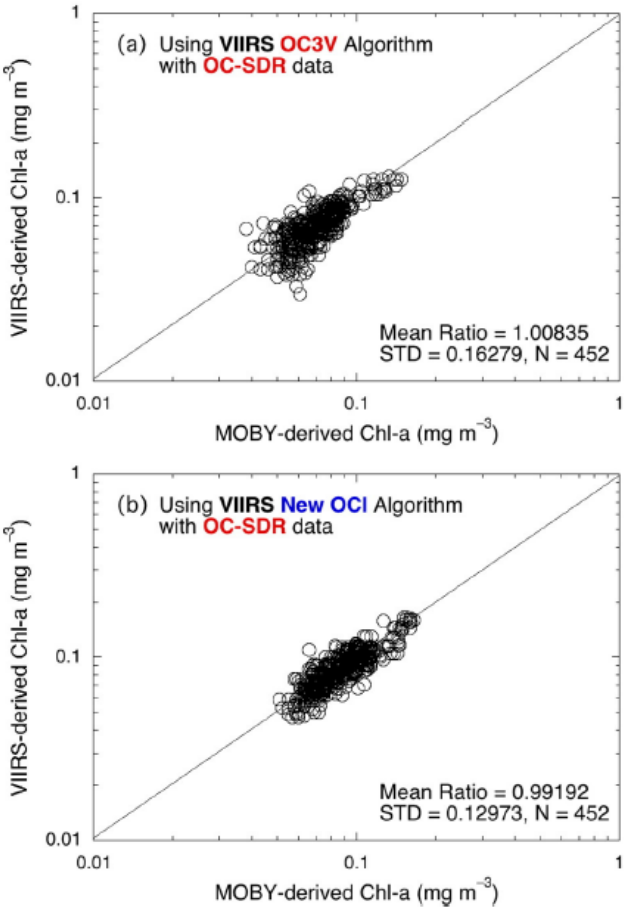

Figure 4. VIIRS-derived Chl-a data compared with those derived from the in situ MOBY optics data using the same Chl-a algorithm of (a) the OC3V and (b) the new OCI algorithm. Note that the improved OC-SDR data were used for generating VIIRS Chl-a data.

Ocean Color - The NIR and SWIR-based atmospheric correction algorithms are used in satellite ocean color data processing with the SWIR-based algorithm particularly useful for turbid coastal and inland waters. In this study, we describe the NIR- and two SWIR-based on-orbit vicarious calibration approaches for satellite ocean color sensors, and compare results from these three on-orbit vicarious calibrations using satellite measurements from Suomi NPP VIIRS. Vicarious calibration gains for VIIRS spectral bands are derived using the in situ normalized water-leaving radiance $nL_w(\lambda)$ spectra from MOBY in waters off Hawaii. The SWIR vicarious gains are determined using VIIRS measurements from the South Pacific Gyre region, where waters are the clearest and generally stable. Specifically, vicarious gain sets for VIIRS spectral bands of 410, 443, 486, 551, and 671 nm derived from the NIR method using the NIR 745 and 862 nm bands, the SWIR method using the SWIR 1238 and 1601 nm bands, and the SWIR method using the SWIR 1238 and 2257 nm bands are (0.979954, 0.974892, 0.974685, 0.965832, 0.979042), (0.980344, 0.975344, 0.975357, 0.965531, 0.979518), and (0.980820, 0.975609, 0.975761, 0.965888, 0.978576), respectively. Thus, the NIR-based vicarious calibration gains are consistent with those from the two SWIR-based approaches with discrepancies mostly within processing methods.

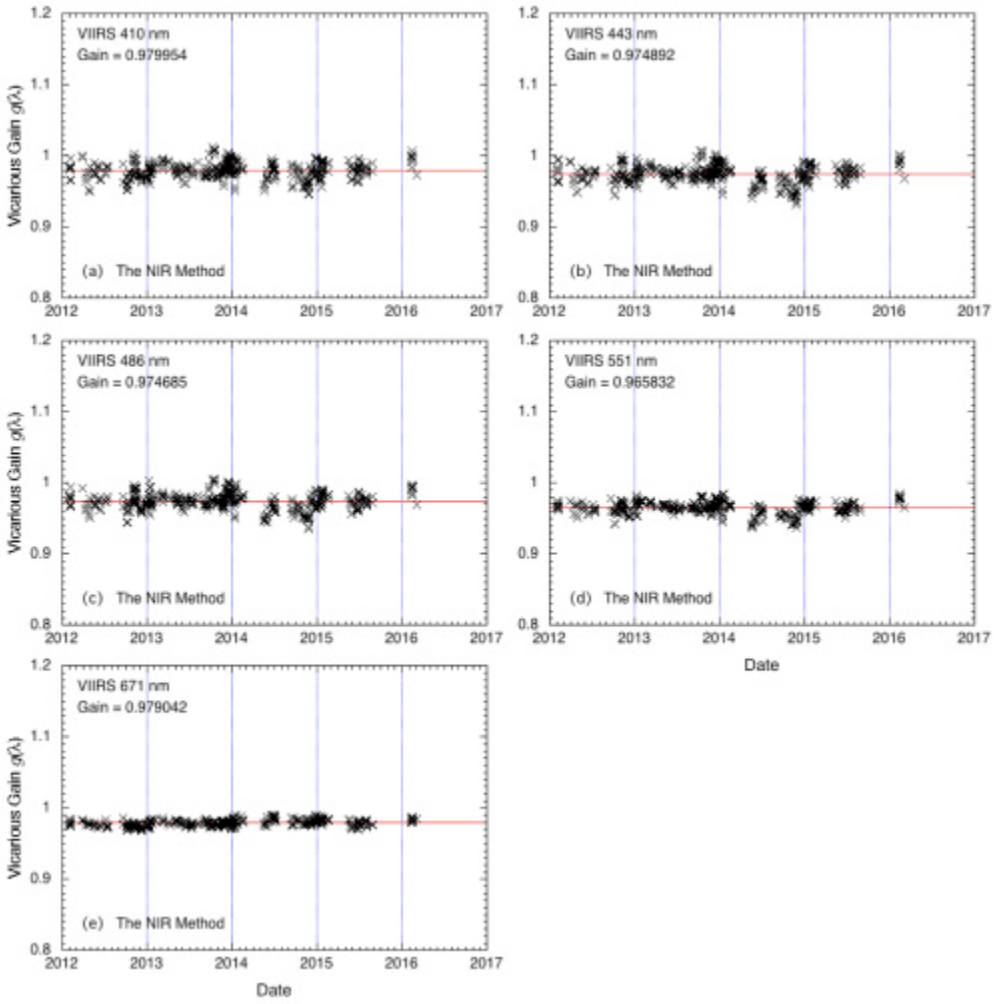

Figure 5. Vicarious calibration gains $g^{(NIR)}(\lambda)$ as a function of time from 2012 to 2016 derived using the NIR-based VC method for VIIRS bands at (a) 410 nm, (b) 443 nm, (c) 486 nm, (d) 551 nm, and (e) 671 nm. For a clear demonstration, $g^{(NIR)}(\lambda)$ values are plotted in every 50 values for each plot.

In addition, the NIR vicarious gains (745 and 862 nm) derived from the two SWIR methods are (0.982065, 1.00001) and (0.981811, 1.00000), respectively, with the difference ~0.03% at the NIR 745 nm band. This is the fundamental basis for the NIR-SWIR combined atmospheric correction algorithm, which has been used to derive improved satellite ocean color products over open oceans and turbid coastal/inland waters. Therefore, a unified vicarious gain set for VIIRS bands M1–M8 and M10–M11 has been implemented in the VIIRS ocean color data processing. Using the unified vicarious gain set, VIIRS mission-long ocean color data have been successfully reprocessed using the NIR-, SWIR-, and NIR-SWIR-based atmospheric correction algorithms.

Ocean Color – Suomi NPP VIIRS satellite that launched from Vandenberg Air Force Base, California, on October 28, 2011. It is a whiskbroom radiometer that provides 56.28° scans of the Earth view. It has 22 bands, among which 14 are reflective solar bands (RSBs). The RSBs cover a wavelength range from 410 to 2250 nm. The RSBs of a remote sensor are usually sensitive to the polarization of incident light. For VIIRS, it is specified that the polarization factor should be smaller than 3% for 410 and 862 nm bands and 2.5% for other RSBs for the scan angle within 45°. Several polarization sensitivity tests were performed prelaunch for SNPP VIIRS. The first few tests either had large uncertainty or were less reliable, while the last one was believed to provide the more accurate information about the polarization property of the instrument. In this paper, the measured data in the last polarization sensitivity test are analyzed, and the polarization factors and phase angles are derived from the measurements for all the RSBs. The derived polarization factors and phase angles are band, detector, and scan angle dependent. For near-infrared bands, they also depend on the half-angle mirror side. Nevertheless, the derived polarization factors are all within the specification, although the strong detector dependence of the polarization parameters was not expected. Compared to MODIS on both Aqua and Terra satellites, the polarization effect on VIIRS RSB is much smaller.

Science and Applications

LST – The team has completed its first collection of in situ data from Chile. There are four in situ data stations maintained by University of Chile, with one of them has four component measurements which can be used for direct in situ LST estimation.

Different cloud filtering scenarios have been applied for the VIIRS LST and the in situ LST comparisons. Further investigation on this in situ data application is ongoing.

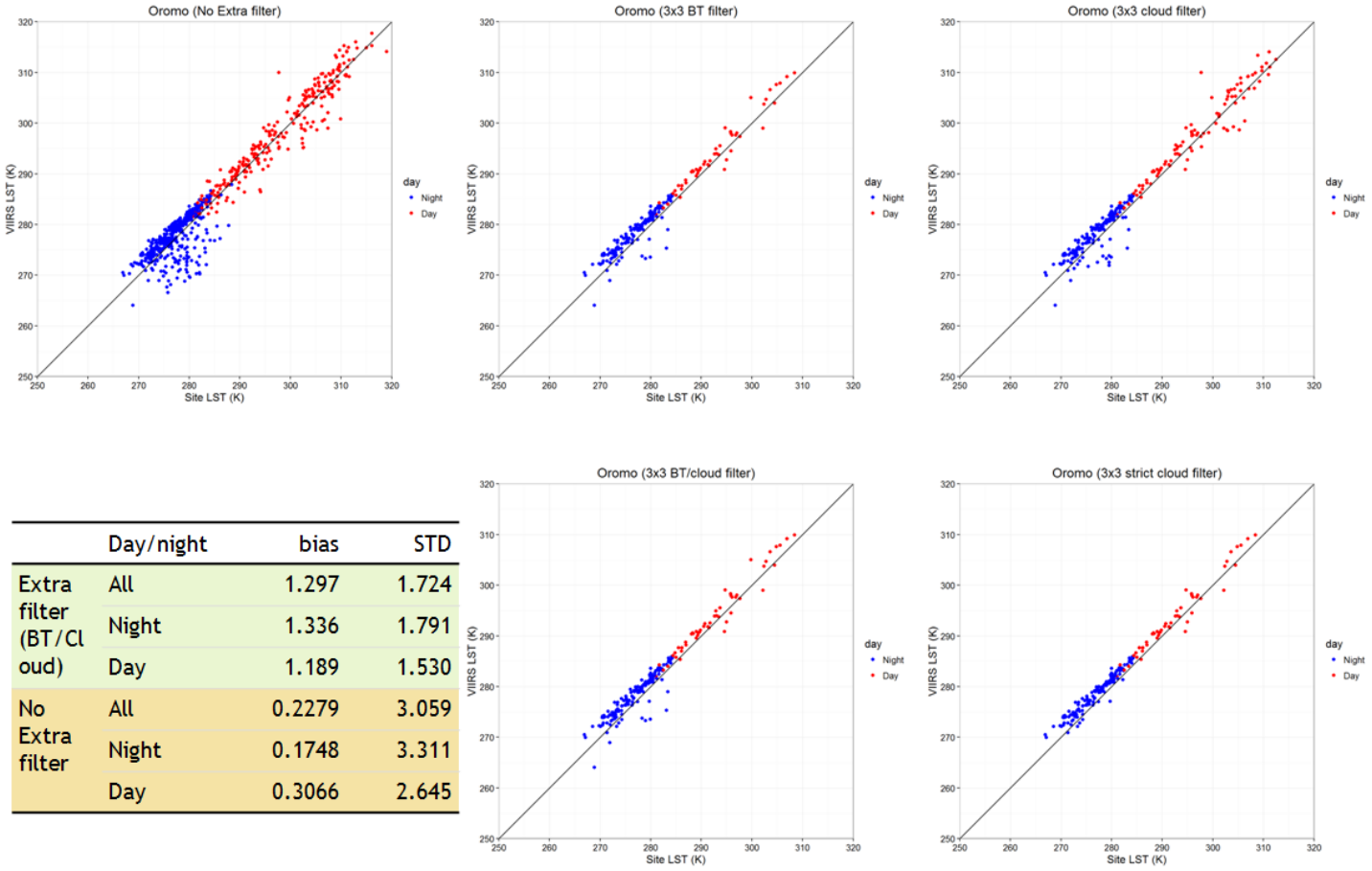

	Day/night	bias	STD
Extra filter (BT/Cloud)	All	1.297	1.724
	Night	1.336	1.791
	Day	1.189	1.530
No Extra filter	All	0.2279	3.059
	Night	0.1748	3.311
	Day	0.3066	2.645

Figure 6. Plots and table of in situ LST evaluation using the ground data collected from Chile. Top-left: no extra cloud filter (i.e. only the VIIRS cloud mask is applied); top-middle: a 3×3 window BT variation filter is applied in addition to the VIIRS cloud mask; top-right: a 3×3 window neighborhood pixel cloud mask is applied; bottom-left: both the 3×3 brightness temperature and the cloud mask filters applied; bottom-right: all the above filters applied.

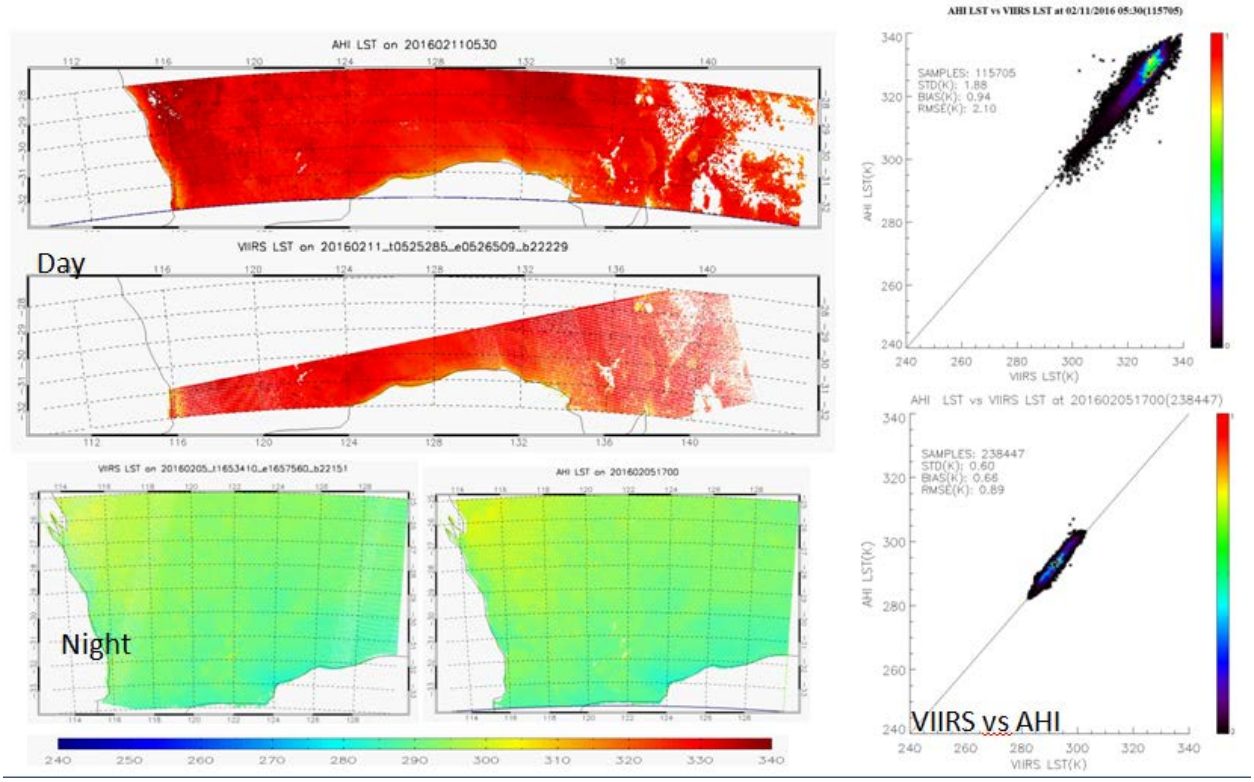

Figure 7. top/middle: daytime VIIRS and AHI LSTs derived using Enterprise LST algorithm; bottom: nighttime VIIRS and AHI LSTs of the Enterprise Algorithm retrieval.

LST - A comparison of the enterprise VIIRS LST and the AHI LST is performed for evaluating the VIIRS and ABI LST product difference.

LST - An investigation has been conducted to find out how the surface broadband emissivity uncertainty will impact the LST derivation. The investigation is done by comparing the broadband emissivity between the in situ estimates and the satellite derivation and statistical LST derivation difference due to the emissivity difference. The table and plots below shows the investigation results

.

	BON	TBL	DRA	FPK	GWN	PSU	SXF	GOB	CAB	SUM
Emis_dif	0.009	0.009	0.038	0.015	0.023	0.015	0.011	0.030	0.010	-0.003
LST_dif	-0.136	-0.168	-0.932	-0.258	-0.317	-0.231	-0.149	-0.698	-0.151	0.044

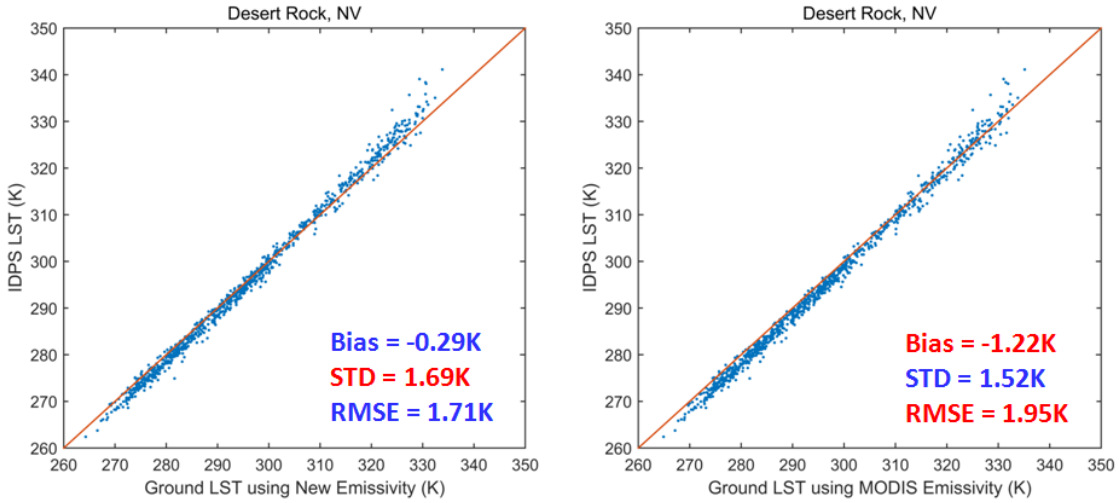

Figure 8 -

MiRS - Tropical Storm Hermine, which briefly intensified to hurricane strength before making landfall, was observed in microwave satellite data from Suomi NPP/ATMS over the Gulf of Mexico on September 1, 2016. The NOAA MiRS retrieved surface rain rates in and around the storm at 1910 UTC (approximately 310 pm local time) as the storm was intensifying just a few hours prior to landfall on the west coast of Florida. As shown in the figure maximum rain rates were estimated to exceed 15 mm/h (0.6 in/h). Comparison with the operational Stage IV radar-gauge analysis at the same time show good qualitative agreement.

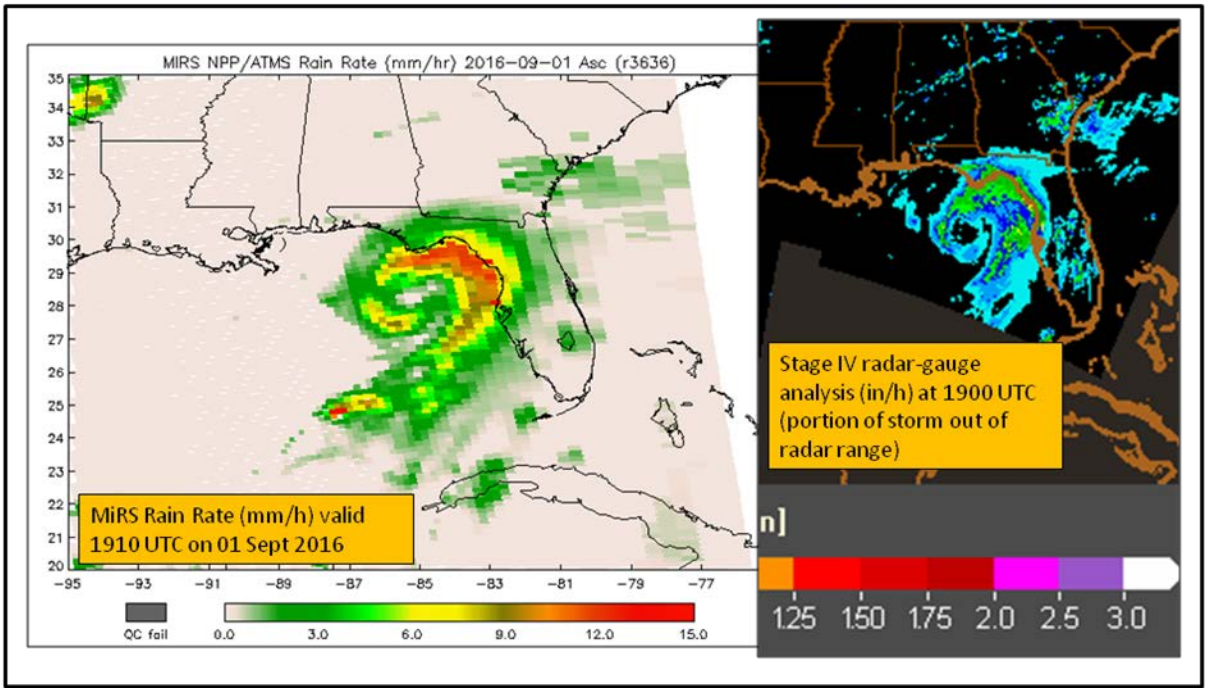

Figure 9. MiRS retrievals of rain rate (mm/h) around Tropical Storm Hermine from Suomi NPP ATMS microwave observations at 1910 UTC on 1 September 2016. Panels show MiRS surface rain rate (left), and Stage IV radar-gauge analysis (right). Maximum MiRS rain rain rates of 15 mm/h correspond to 0.6 in/h, in agreement with Stage IV.

Surface Type - The team successfully retrained a new classification model using the 2015 annual metrics and training polygons collected last year. The new model was used to classify the 2015 annual metrics and a SVM classification map was obtained. The result is visually checked, and it is found that higher quality is achieved using the new annual metrics. The team is performing the post-classification processes over the initial classification result to further improve the quality and accuracy of the 2015 surface type classification map. A post-processed global surface type map based on 2015 data will be delivered at the end of this month.

Clouds - Low clouds develop commonly over warm ocean accompanied with temperature inversion. Under this situation, NOAA's cloud height retrieval algorithm (ACHA) derives cloud top height by dividing the temperature difference ΔT by an effective lapse rate in-between. Here ΔT refers to difference between the retrieved cloud temperature from the OE algorithm and surface temperature interpolated from the NWP fields. This is generally applied to water phase clouds over non-snow covered water surfaces. However, it can be problematic along the coast, or wherever transition between land and water occurs, treating the same broad-covered low clouds using different techniques. The figure shows an example over the west coast near San Francisco Bay where low clouds drift towards inland and ACHA reports a dramatic contrast in cloud height. It is confirmed by Figure 2 that the cloud top should be located around similar levels as seen from the homogeneous cloud temperature field. As a result, a new look-up-table of lapse-rate constants was derived for land area under inversion conditions and integrated into ACHA. Figure 3 demonstrates the significant improvement for inland cloud top height. This also improves other products that directly depend on cloud top height, such as the cloud base height. Additionally, studies using one day of global data suggest a modest improvement in retrieved cloud height by comparing against CALIPSO.

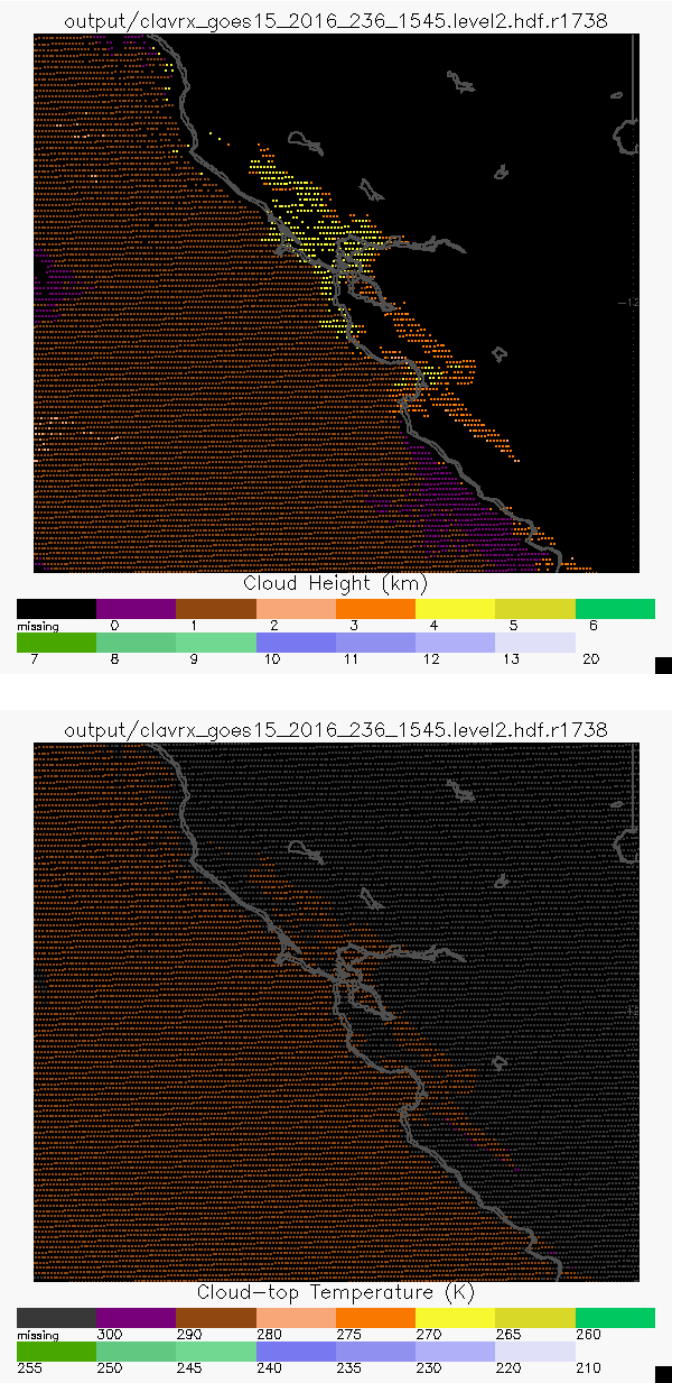

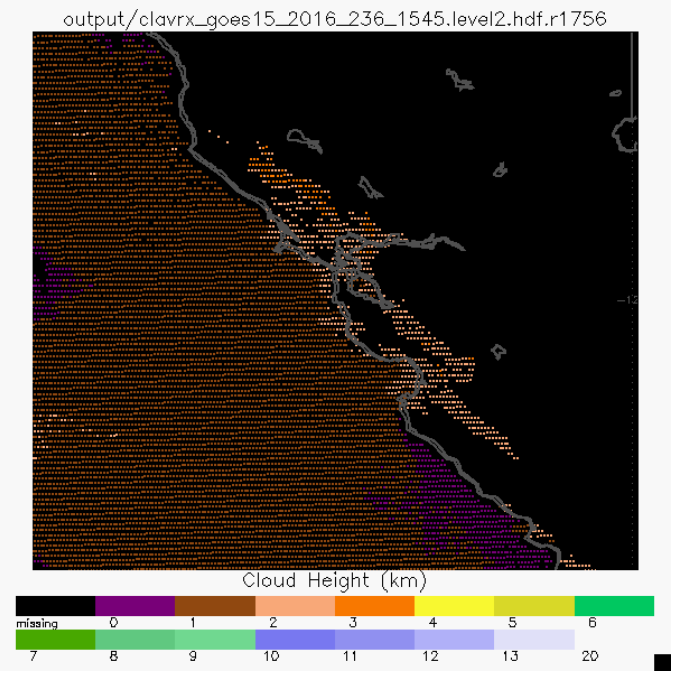

Figure 10. A granule shows ACHA retrieved cloud top height near San Francisco Bay. Values over ocean are estimated from the lapse rate method, whereas over land the NWP profiles are used.

The same granule as above shows the cloud top temperature, a direct retrieved variable from ACHA OE algorithm.

The same granule as Figure 1. shows estimated cloud top height after applying lapse rate method to near-water land area under inversion conditions.

Imagery - Imagery provided by RAMMB/CIRA was used extensively in the media's coverage of Super Typhoon Meranti that skirted the southern coast of Taiwan this week. Here are some select articles that included both Himawari and VIIRS imagery from RAMMB/CIRA:

http://mashable.com/2016/09/13/typhoon-meranti-strongest-storm-taiwan/#Im5sitRAIaqD ,
https://weather.com/storms/typhoon/news/super-typhoon-meranti-satellite-images ,
http://nymag.com/daily/intelligencer/2016/09/this-is-2016s-biggest-storm-so-far.html ,
http://nymag.com/daily/intelligencer/2016/09/this-is-2016s-biggest-storm-so-far.html ,
https://www.washingtonpost.com/news/capital-weather-gang/wp/2016/09/13/7-images-of-super-typhoon-meranti-the-strongest-storm-on-earth-in-2016/ . Some of the Himawari loops were also shown on a number of TV stations.

The figures below are images of the wildfire near Vandenberg AFB in California. See the figure captions for details.

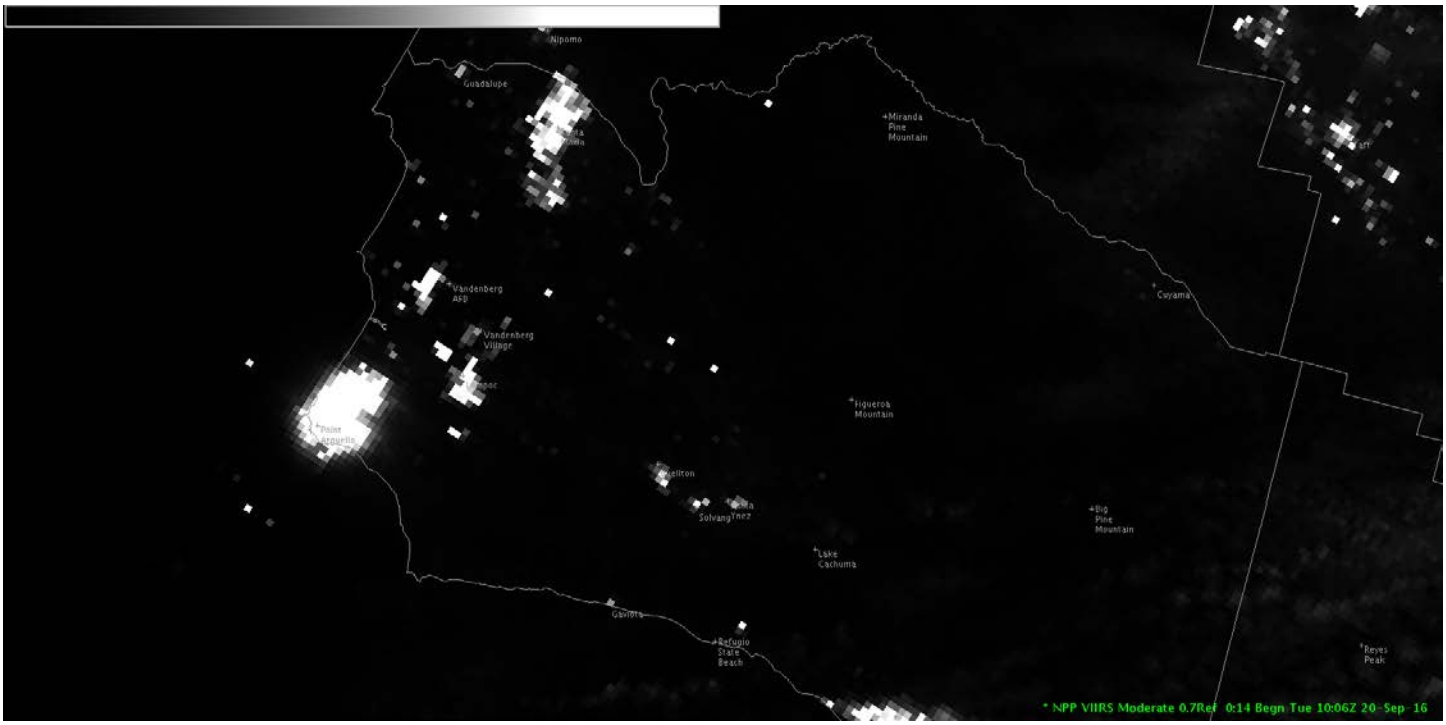

Figure 11. Nighttime NCC Image from September 20, 2016 at 1006 UTC, at about the height of the Vandenberg AFB wildfire at the southwest tip of the land near Point Angelo. At later times the fire decreased in intensity/brightness.

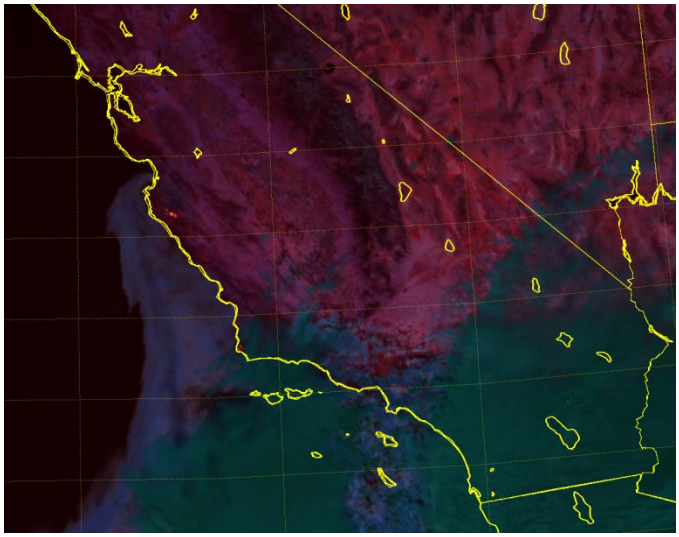

Figure 12. VIIRS Fire Temperature RGB product, showing a bright red spot near Point Angelo on September 19, 2016 at 2010 UTC. This image also shows a fire farther up the coast, south of Monterrey CA and near Big Sur.

A new VISIT Blog, titled 'Puerto Rico Power Outage' can be found at http://rammb.cira.colostate.edu/training/visit/blog/. Excerpted images are attached.

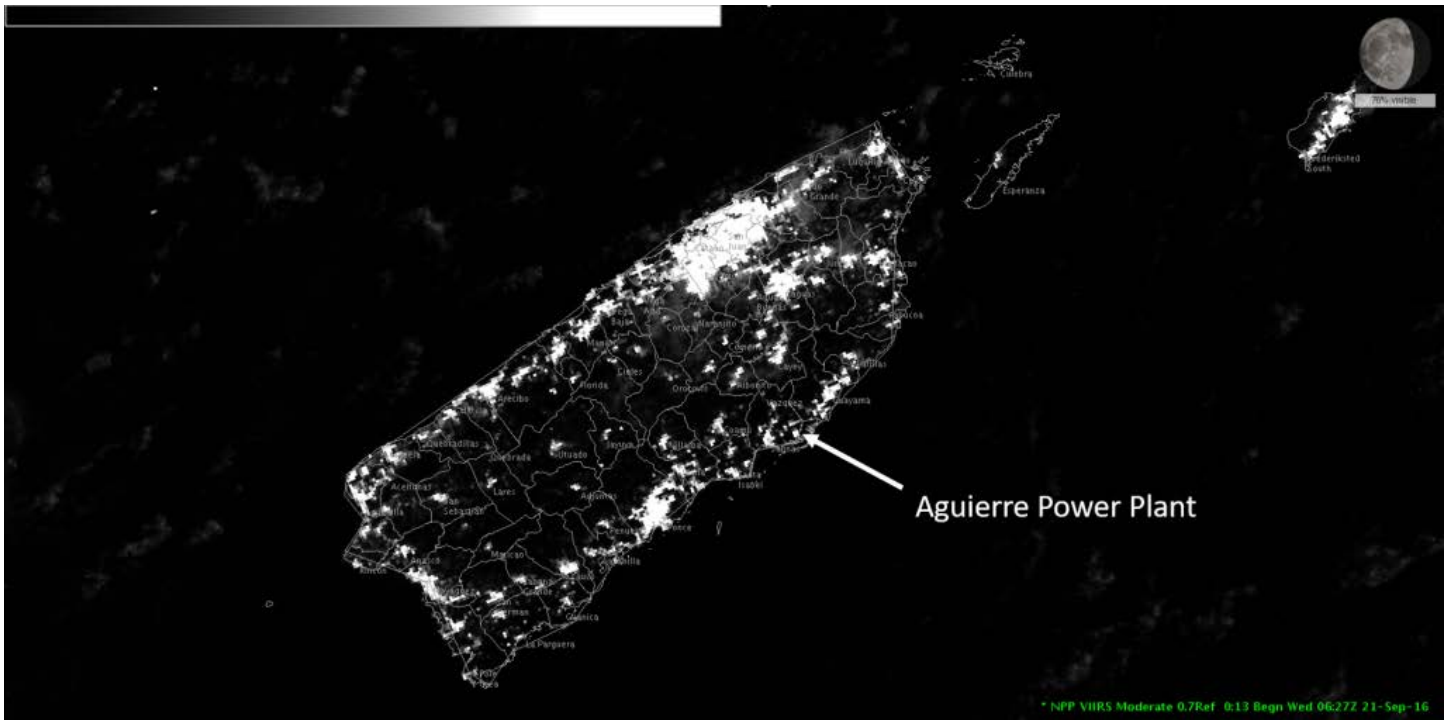

Figure 13. The NCC product highlighting the emitted lights from cities and towns on the island of Puerto Rico. The satellite image is taken on September 21, 2016 @ 0627 UTC before the power outage occurred. The Aguierre Power Plant where the fire first started and took out the power-grid in Puerto Rico is also seen. In the top-right corner of the figure one can see the approximate moon phase of the lunar cycle, where there is a correlation between the distinct satellite imagery and moon phase.

Figure 14. The NCC product shows the decrease in emitted light from cities and towns on the island of Puerto Rico on September 22, 2016 @ 0608Z after the power outage occurred. In the top-right corner of the figure one can see the approximate moon phase of the lunar cycle.

A new VISIT Blog, titled 'Puerto Rico Power Outage' can be found at http://rammb.cira.colostate.edu/training/visit/blog/. Excerpted images are attached.

Meetings and Reviews

Aerosols - The NOAA STAR aerosol team organized a two-day workshop on September 13-14, 2016 and conducted briefings and interactive hands-on tutorials for science and operational users. Over 70 participants from the NWS, EPA, NASA, NRL, academia, and several state and local environmental agencies attended the workshop. Status of the new algorithms and maturity of various aerosol products along with visualization tools was presented and well received. Operational air quality forecasters presented specific case studies of air quality standard exceedances as example to demonstrate how they use satellite aerosol products in their day to day forecasting activities. Scientists representing agencies that provide aerosol forecast guidance (e.g., NRL) presented their progress on Suomi NPP VIIRS aerosol assimilation activities. The workshop also had a productive breakout round-table discussion on some topical issues of aerosol remote sensing and policy relevant applications.

LSA - The Enterprise LSA Algorithm development Critical Design Review is scheduled in this month. Slides of the algorithm theoretical base have been written, in which a 2-step LSA algorithm is described. The 2-step algorithm includes an online process and offline process. The online process first computes a primary granule LSA data similar to the current IDPS LSA product and then run a temporal filtering process using historical LSA and the primary LSA data. The offline process runs temporal filtering using daily primary data, historical data and climatology data. The processing flowchart is shown below.

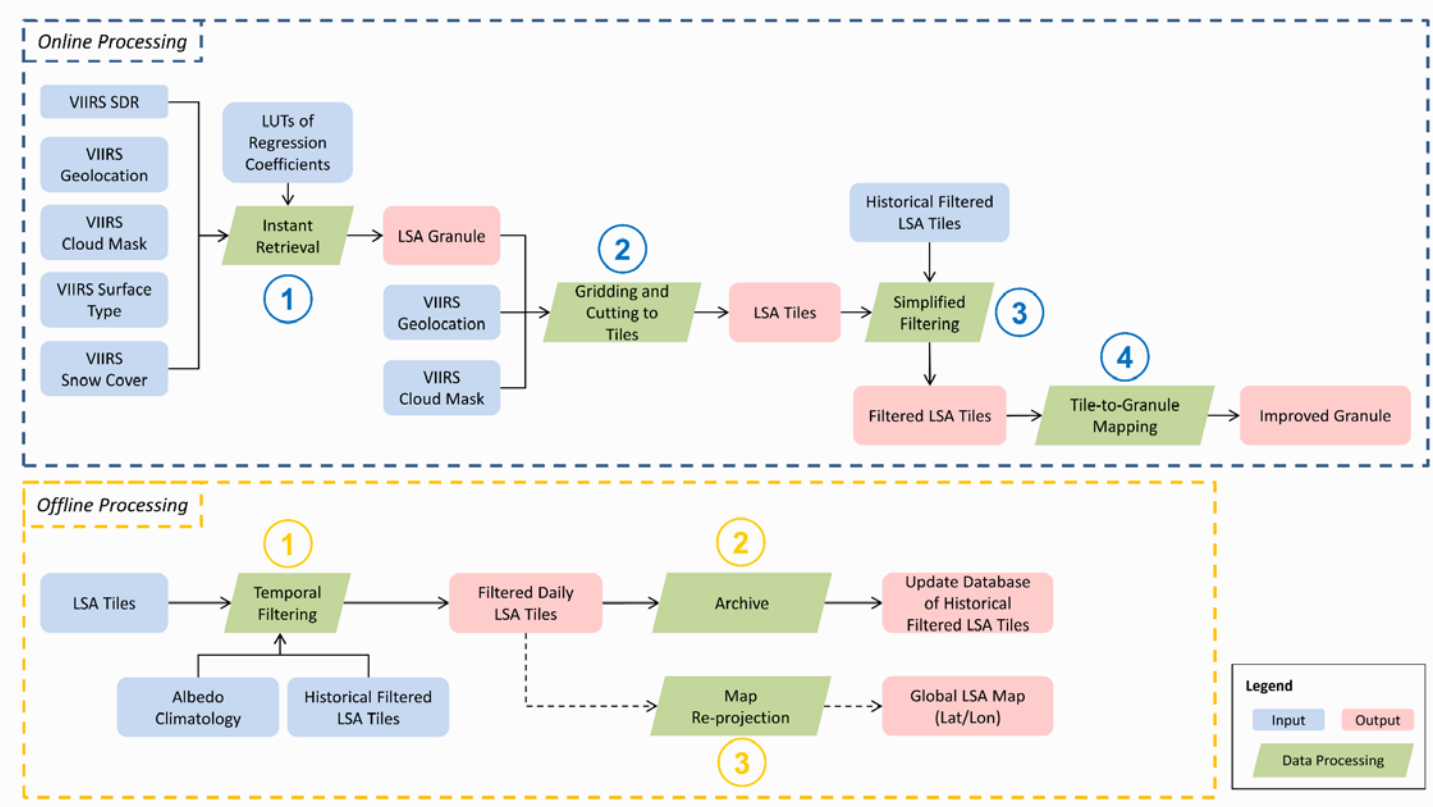

Figure 15.

GCOM - OSPO conducted an operational readiness review for the Day-2 (Snow, Ice, Soil Moisture) GCOM AMSR-2 EDR's on August 26, 2016. Aside from a few minor comments, the review was successful and OSPO plans to have the products operational by September 30.

VIIRS - STAR VIIRS SDR team members actively participated in SPIE conference (San Diego, Aug. 28- Sep. 01, 2016) with following presentations:

- S-NPP VIIRS thermal emissive band gain correction during the blackbody warm-up-cool-down cycle
- Trade study of substituting VIIRS M10 with aggregated I3 to enable addition of a water vapor channel and
- Influence of atmospheric turbulence on the visible infrared imaging radiometer suite (VIIRS) day/night band (DNB) low light calibration with ground based light source
- "Joint Polar Satellite System-1 (J1) Visible Infrared Imaging Radiometer Suite (VIIRS) at-launch geometric performance" and
- "Trending of Suomi National Polar-orbiting (SNPP) ephemeris and its implications on VIIRS geometric performance".

NUCAPS - Participated in the NASA Sounder Science Team Meeting, 13-16 September 2016. Prepared and gave an oral presentation entitled "

- "Estimation of outgoing longwave radiation from Cross-track Infrared Sounder radiance measurement"
- "Atmospheric Stability Indices Derived from Temperature and Water Vapor Retrieved from Satellite Observations using NUCAPS CrIS/ATMS"
- "Retrieval of Atmospheric Methane (CH4) using S-NPP CrIS Full Spectral Resolution Data"

- "Satellite Sounder Observations of Contrasting Tropospheric Moisture Transport Regimes: Saharan Air Layers, Hadley Cells, and Atmospheric Rivers"
- "NUCAPS Atmospheric Profile EDR Performance: Ozone and Carbon Trace Gases"

Anomalies, Monitoring, and Discrepancy Reports

CrIS - Team members from the Space Dynamics Laboratory and STAR reported recent findings of SDR anomaly events associated with the Southern Atlantic Anomaly activates. The uniqueness of the August 19, 26, and 27, 2006 events is that they are not single events that affect only one spectrum at a time, but continue over multiple scans, which is an indication that the high energy particles hit the electronics.

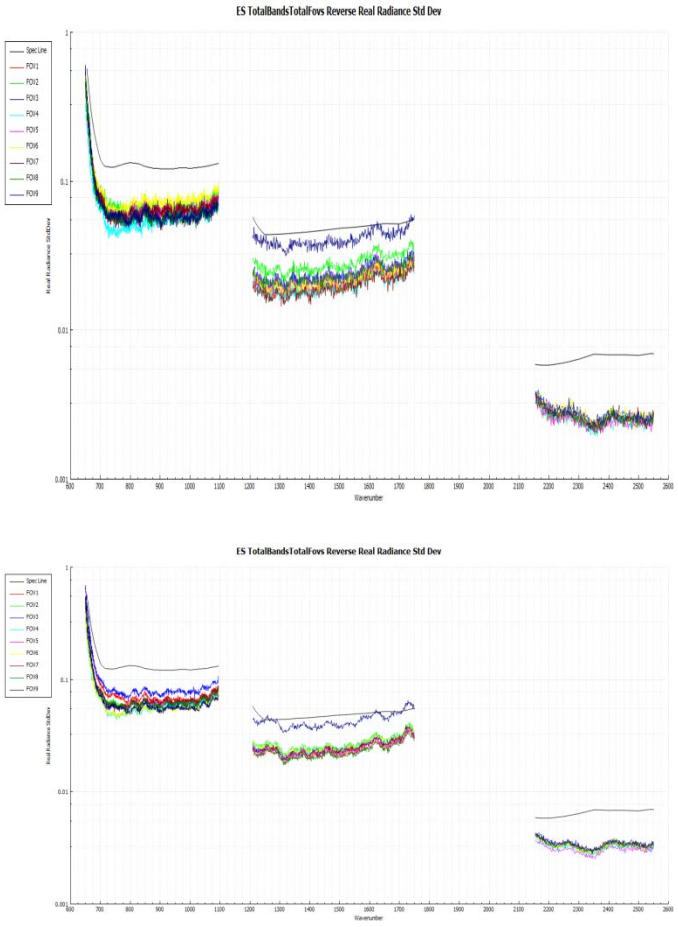

Figure 16. (top) NEdN from the J1 S/C level TVAC test; (bottom) NEdN from the previous J1 instrument level TVAC test.

Team members from UMBC and UW presented investigation results on the LW FOV-5 cold scene anomaly near 668 cm^{-1} (see Figures CrIS-2 and CrIS-3). Presentations focused on the possible causes. No conclusion was made. The investigation is ongoing.

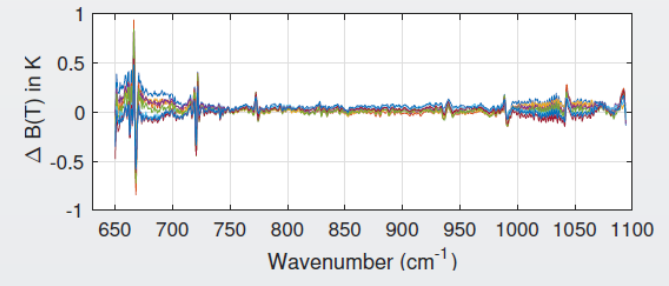

Figure 17. CrIS FOV5 brightness temperature showing the spikes near 668 cm^{-1} and 720 cm^{-1}

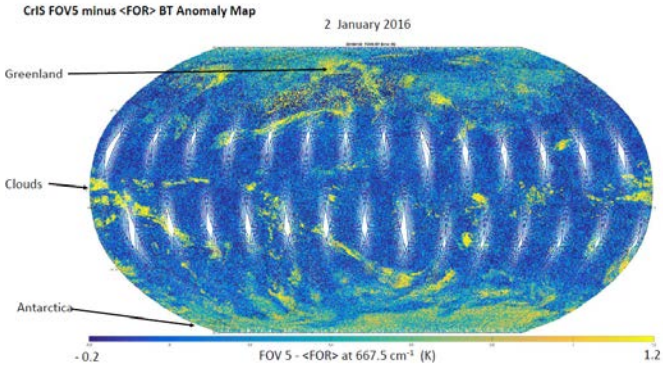

Figure 17. LW band FOV-5 668 cm^{-1} cold scene anomaly over deep convective clouds, Greenland and Antarctic.

Imagery - D. Hillger and R. Marley started the Discrepancy Reporting process to change the geo-locations for VIIRS EDR Imagery from ellipsoid to terrain-corrected. This was motivated by feedback from users who noticed that city lights moved from night-to-night (image-to-image), particularly at higher elevations) in loops created of NCC Imagery that were used to track wildfires in both Colorado

and California. (NCC Imagery has been available on AWIPS to NWS users since December 2015.). The image movements are on the order of several kilometers, due to the fact that the viewing angle for the same location varies from image to image. As a clue to the source of the problem, the same imagery loop created from DNB (with terrain-corrected geo-locations) has stable city lights, and is better able to follow actual movement/changes in wildfires without having to endure shifts in the imagery due to navigation errors. The same change in geo-location type was previously made to (SDR) DNB Imagery in the 2013/2014. The new Discrepancy Report is ADR 8239 (Imagery) - Terrain-Correction geo-locations needed for VIIRS EDR Imagery.

Imagery - VIIRS EDR Terrain-Corrected geo-location progress: The Imagery Team is now working with Weizhong Chen at ASSISTT (who already works with the VIIRS SDR and Cloud Teams) to set up test cases that can be run on ADL. The output from that test run (or runs) will be sent to the Imagery Team to analyze the impact of the change from ellipsoid geo-locations to terrain-corrected geo-locations. The Imagery Team in particularly interested in lessening the artificial movement in nighttime lights, as well as well as visible and IR features, at higher elevations where the terrain-corrected geo-locations used by VIIRS SDRs are clearly better than the ellipsoid geo-locations used by VIIRS EDRs. It appears neither the L1 documentation or the SRS contain any explicit statement what geolocation the Imagery EDR should be using, which greatly reduces the documentation headaches surrounding this change.

Imagery - W. Ibrahim started the ADR process to deal with EDR geo-location issues related to spacecraft maneuvers. Noted as ADR 8251 (Imagery) - VIIRS Imagery EDR/GTM GEO Issues During Maneuvers, however the DRAT decided to proceed with ADR 8196 instead, which is the related ADR from the GEO team that Gary Lin brought up during the DRAT meeting. ADR 8196 was approved for a post- J1 launch code change. This code change will use a scan level quality flag to mask the GEO products with fills during spacecraft maneuvers. Once this code change is implemented, we will see if it resolves the issue at hand. If not, ADR 8251 will be brought back into play. (W. Ibrahim, Raytheon)

VIIRS - Attended J2 Tech Issues Telecon. Discussed scan-to-scan underlap and possible paths forward. Discussed DNB underlap. Calculated the J1 and J2 DNB underlaps (Fig. VIIRS-2):

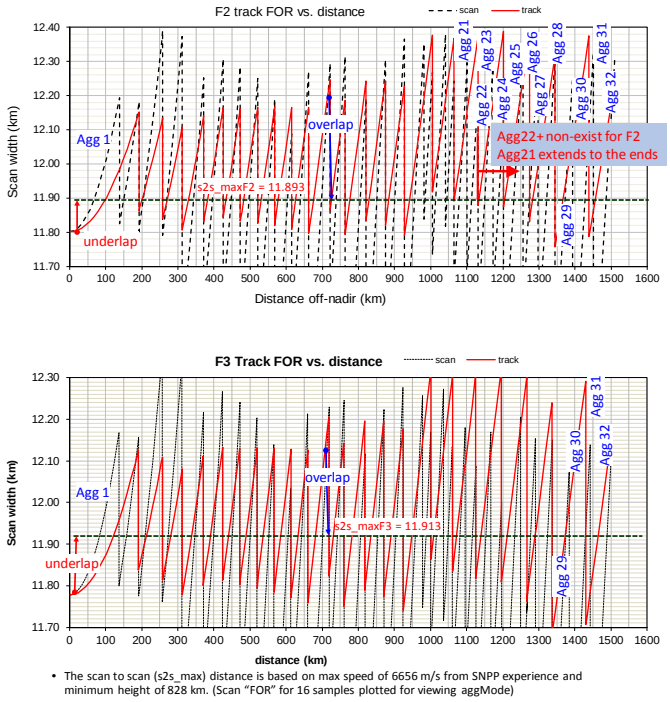

Figure 17. VIIRS DNB scan-to-scan underlap (upper for J1 F2 and lower for J2 F3) over the equatorial regions.

CriS - SDL collected data set with 173 FCE events recorded on September 5 during the temperature transition to a cold balance. An example of the phase shift due to FCE is shown in Figure CrIS-1. The data sets are valuable for testing the new FCE handling algorithm recently implemented in the operational code. So far the FCE events haven't been observed in balanced environment and in space. SDL also showed J1 CrIS NEdN performance with the expected results, consistent with the early Vendor TVAC data analysis.

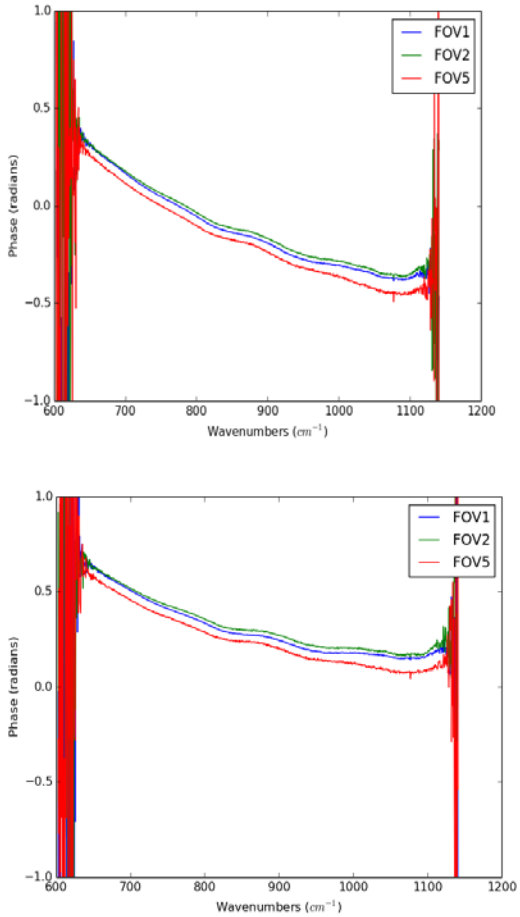

Figure 18. Phase shift between scan 2 (left) and scan 3 (right) due to Fringe Count Error (FCE)

CrIS - Harris presented updated J1 spacecraft level TVAC analysis, including NEdN from both Hot and Cold environments. An example of the modeled and measured NEdN is shown in Figure CrIS-2. The results are expected. Harris also showed FCE events recorded on September 9. The data with the FCE errors were processed by Harris SDR software. The LW band showed that the FCE algorithm works fine, but the MW and SW bands showed the algorithm does not work well. Harris is looking into the issue.

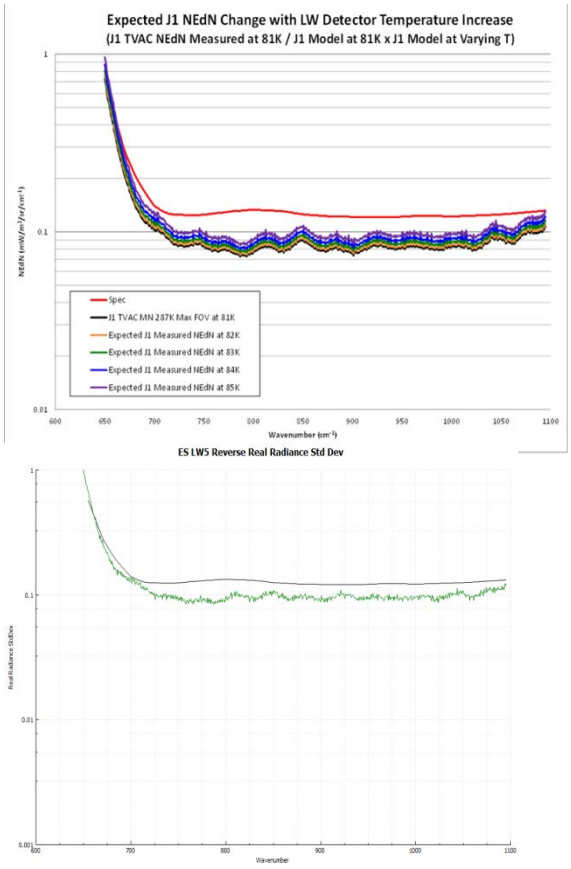

Figure 19. modeled maximum LW band NEdN (left) and measured LW5 NEdN for 84 K detector temperature.

VIIRS - VIIRS Scan-to-Scan Underlap meeting: D. Hillger and S. Kidder from the EDR Imagery Team provided materials and participated in a special meeting held on 15 September 2016 to discuss the Scan-to-Scan Underlap issue with VIIRS on J1 and J2. As a result of the meeting M. Goldberg will make a formal response to J. Gleason, indicating that the impact is not considered great enough to make high risk changes to VIIRS, but that changes to the orbit be made to compensate for the potential gap between scans, without impacting the 16-day repeat cycle or the 50-minute satellite separation.

VIIRS - STAR VIIRS SDR team used MODIS geolocation products to evaluate scan-to-scan overlap in MODIS data. Despite local variations introduced by terrain correction of the geolocation data, the analysis shows that the scan underlap (negative overlap) in the Terra MODIS data is similar to the one currently predicted for JPSS-1 and JPSS-2 VIIRS: around 100 m in the worst case near 15°N. For Aqua MODIS, the worst case

underlap additionally changes every other scan between approximately 50 m and 150 m, likely due to a scan mirror misalignment. This study helps understand effects of the potential VIIRS scan underlap on the future JPSS science products.

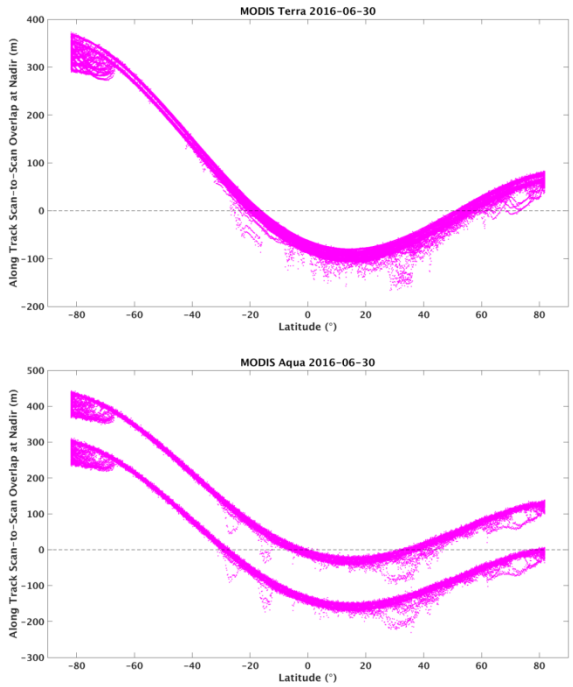

Figure 20. Along track scan-to-scan overlap at nadir for MODIS Terra (top) and Aqua (bottom) measured between all scans using geolocation data from June 30, 2016.

VIIRS - Team members from the NASA VCST-Geometric sent out updated plots of the trends in Suomi NPP VIIRS RTA/HAM sync losses (Fig. VIIRS-2) after learning new events #65 on 9/3/2016 22:23:36 – 22:25:04 UTC and #66 on 9/13/2016 9:50:21 – 9:52:00z.

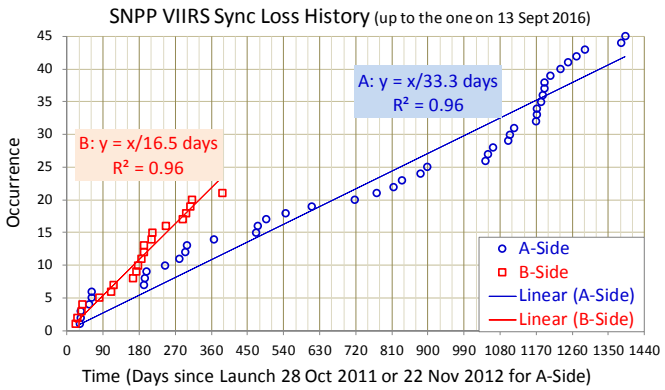

Figure 21. Trend of Suomi NPP VIIRS RTA/HAM sync losses.

VIIRS - Aerospace VIIRS SDR team analyzed the DNB portion of RSBAutocal and discovered gain ratio instability in 25% of LGS-to-MGS detector/agg zone combinations and 40% of LGS-to-HGS detector/agg zone combinations. To analyze gain ratio instability, we have developed a Matlab version of DNB RSBAutocal, as it is much easier and takes less time/storage to run large amounts of DNB data through Matlab vs. ADL. Due to the way dark signal is calculated in RSBAutocal, small perturbations in dark signal (0.5DN) lead to much larger changes in gain ratio. Through the Matlab model, we have developed a solution to mitigate the gain ratio instability which will lead to turning the DNB portion of RSBAutocal into automated mode. The full solution requires LUT changes as well as multiple code changes. We are running trade studies to determine the effects of each code change.

Acronym Index

ABI - Advanced Baseline Imager
ACAPEX - ARM Cloud Aerosol Precipitation Experiment
ACHA - ABI Cloud Height Algorithm
ADL - Algorithm Development Library
ADR - Algorithm Discrepancy Report
AEROSE - Aerosols and Ocean Science Expeditions
AFB - Air Force Base
AGU - American Geophysical Union
AHI - Advanced Himawari Imager
AIT - Algorithm Integration Team
AMS - American Meteorological Society
APP-x - Extend AVHRR Polar Pathfinder
ARM - Atmospheric Radiation Measurement
ATMS - Advanced Technology Microwave Sounder
AVHRR - Advanced Very High Resolution Radiometer
AVMP - Atmospheric Vertical Moisture Profile
AWIPS - Advanced Weather Interactive Processing System
Chl-a - chlorophyll-a
CI - color index
CICS - Cooperative Institute for Climate and Satellites
CIMSS - Cooperative Institute for Meteorological Satellite Studie
CIRA - Cooperative Institute for Research in the Atmosphere
CrIS - Crosstrack Infrared Sounder

DNB - Day/Night Band
EDR - Environmental Data Record
EPA - Environmental Protection Agency
FCE - fringe count error
FOV - field-of-view
GCOM - Global Change Observation Mission
GOFC-GOLD - Global Observation of Forest and Land Cover Dynamics
GTM - Ground Track Mercator
HAM - half-angle mirror
HGS - high gain stage
ICESat - Ice, Cloud, and Land Elevation Satellite
IMSG - IM Systems Group
J1 - JPSS-1
JGR - Journal of Geophysical Research
JPL - Jet Propulsion Laboratory
JPSS - Joint Polar Satellite System
LGS - low gain stage
LSA - land surface albedo
LST - land surface temperature
LW - longwave
MIRS - Microwave Integrated Retrieval System
MOBY - Marine Optical Buoy
MODIS - Moderate-resolution Imaging Radiometer Suite
MSL12 - Multisensor Level 1 to 2
MW - midwave
NASA - National Aeronautics and Space Administration
NCC - Near Constant Contrast
NDE - NPP Data Exploitation
NIR - near infrared
nL_w - net water-leaving radiance
NOAA - National Oceanic and Atmospheric Administration
NPP - National Polar-orbiting Partnership
NRL - Naval Research Laboratory
NUCAPS - NOAA Unique CrIS/ATMS Processing System
NWP - numerical weather prediction
NWS - National Weather Service
OCI - Ocean Color Index
OCx - ocean chlorophyll type
OSPO - Office of Satellite Products and Operations
PIOMAS - Pan-Arctic Ice-Ocean Modeling and Assimilation System
RAMBB - Regional and Mesoscale Meteorology Branch
RGB - red-green-blue
RTA - rotating telescope assembly
S/C - spacecraft
SDL - Space Dynamics Laboratory
SDR - Sensor Data Record
SMOS - Soil Moisture and Ocean Salinity
SRG - Systems Research Group, Inc.
STAR - Center for Satellite Research and Applications
SVM - Support Vector Machine
SWIR - shortwave infrared
TVAC - thermal vacuum
UMBC - University of Maryland, Baltimore County
UMD - University of Maryland
UTC - Universal Coordinated Time
UW - University of Washington
VC - vicarious calibration
VCST - VIIRS Calibration Support Team
VIIRS - Visible Infrared Imaging Radiometer Suite